Oxide Dispersion Strengthened Steels for Advanced Blanket Systems*)

Akihiko KIMURA, Wentuo HAN, Hwanil JE, Kiyohiro YABUUCHI and Ryuta KASADA

Institute of Advanced Energy, Kyoto University, Uji 611-0011, Japan

(Received 13 December 2015 / Accepted 19 April 2016)

Oxide dispersion strengthened (ODS) steels with nano-scaled oxide particles in high density in ferrite/martensite matrix and on grain boundaries of ultra-fine grains have excellent properties as structural material for fusion blankets, while some issues of fabrication processes are still remaining to be solved. In this overview, material properties of recently developed ODS steels are introduced in comparison to ferritic/martensitic (F/M) steels: 1) mechanical properties, 2) corrosion behavior and 3) radiation tolerance in ODS steels, which are outstandingly superior to the F/M steels. Coupling use of the ODS and F/M steels is effective to expand the design margin of fusion blankets. R&D of dissimilar joining of FM/ODS steels is indispensable.

Keywords: structural material, strength, corrosion, radiation tolerance, high thermal efficiency, long lifetime

DOI: 10.1585/pfr.11.2505090

1. Introduction

Reduced activation ferritic/martensitic (RAFM) steels have been considered to be a candidate of structural material for fusion blanket because of their maturity in manufacturing products and balanced materials properties [1–5]. The sound properties of ferritic/martensitic (F/M) steels is due to the complex martensitic structure including dislocations in high density, lath boundaries, packet boundaries and fine carbides which provide a number of trapping sites for point defects and their clusters [6–8].

International Thermonuclear Experimental Reactor (ITER) blanket module testing is planned to qualify the integrity of candidate blanket concepts and structures. Together with the blanket development, material development is being performed on a prime candidate material that is RAFM steel, and on silicon carbide composite (SiCf/SiC) [9–11], vanadium alloy [12–14] and ODS ferritic steel [15–17] as next stage structural materials for advanced blankets. The RAFM steels were chosen as the structural material of test blanket modules (TBM) of the ITER by all the participating parties. The most of the reasons of the selection of the material other than the other candidates is the maturity of the steel production including manufacturing technology and infrastructure as well as the balanced materials performance.

However, the RAFM steels have still limits of operation conditions as structural materials for the advanced blanket systems with high thermal efficiency and long lifetime in DEMO reactors. Because of the demands of the society to accelerate the development of fusion energy, a target of operation condition of the Japanese solid breeder water cooling DEMO blanket is set for a conservative design using the RAFM steels.

Oxide dispersion strengthened (ODS) steels have been developed for application to fuel claddings of fast reactors [18–25] where high performance materials properties are required to meet the severer conditions of in-core environment such as high doses of neutron irradiation at high temperatures. The ODS steel consists of a number of nano-scaled fine oxide particles in the matrix of the RAFM steel, and resultantly, the trapping sites for radiation defects increase with the number of the particles in comparison to the RAFM steel since the oxide particles/matrix (P/M) interfaces also play a role of trapping defects induced by irradiations [26]. The oxide particles also work as obstacles to dislocation motion providing strain field at the P/M interfaces, which results in the strengthening of the steel at elevated temperatures. As for compatibility issue, high-Cr ODS steels have much better corrosion resistance in a supercritical pressurized water than the RAFM steels [27].

Although the ODS steels show excellent performance as structural material, the steels are produced by means of powder metallurgy processing that gives a limitation of the fabrication of large products. It is considered that the coupling utilization of RAFM and ODS steels is effective to expand the design margin of blankets where the ODS steels are placed in severer environment and the RAFM steels are used for large components in mild environment.

In this overview, the ODS steels R&D for both fusion as well as fission applications is introduced to show their excellent materials performance. The impacts of the achievement of the materials innovations of the ODS steels can give an insight into the advancement of the current con-

author's e-mail: kimura@iae.kyoto-u.ac.jp, wt-han@iae.kyoto-u.ac.jp, hi-je@iae.kyoto-u.ac.jp

*) This article is based on the presentation at the 25th International Toki Conference (ITC25).

servative blanket design to a certain higher level meeting the anticipated demands of the society.

2. ODS Steels

The high strength at elevated temperatures of the ODS steels is due to the fine microstructure that consists of a high number density of nano-scaled oxide particles (~5 nm) and very fine grains (~ 0.5 μm) as well as dislocations in high density.

The chromium (Cr) content in the previous ODS steels is in the range of 9 ~ 19 wt.%, while the content of the other alloying elements (Al, W, Mo, Nb, Ti, Zr etc.) are at a level of a few percent or less, while some of them are excluded from alloy elements for fusion application because of radio activation. The most popular oxide particle of the ODS steels is Y_2O_3 with a size smaller than 10 nm of diameter mostly added with up to 0.5 wt.% at most. Along with yttrium oxides, the alumina [28] and titania [29] were also used.

At present there is a great variety of ODS steel with different grade and type, as grouped according to developer countries (Table 1). Also, it can be categorized into 3 groups as 9Cr-martensitic, 12Cr-ferritic/martensitic and 14(15)Cr-ferritic ODS steels.

3. Mechanical Properties

3.1 Tensile stress

High strength at elevated temperatures of the ODS steels was obtained through refinement of microstructures including a high number density of small Y_2O_3 and TiO_2 particles dispersed in a complex ferrite/martensite matrix [30, 31]. The ODS steels for structural components in fusion reactor would allow an increase in the operation temperature to approximately 650 °C or more [32]. Therefore, the ODS steels are widely considered to be promising candidates for structural materials of fusion reactors as well as the cladding of the next generation fast reactors.

In order to meet the different requirements in the nuclear systems, various ODS steels have been fabricated in Japan, Europe and the United States. Figure 1 shows the tensile results of some of the ODS steels (open symbols) in comparison with the other F/M steels (closed symbols). It can be found that the ODS steels show much higher tensile stresses at all the test temperatures than the non-ODS steels such as F82 H. According to the type of the ODS steels, the tensile properties are ranging over a wide variety of strength level, which is due to the difference in the morphologies of oxide particles, such as, size distribution and the number density as well as the grain size and grain shape among these ODS steels. Until now, many related works have been done to investigate the factors controlling tensile properties. From Fig. 1, it can be said that the upper limit of operation temperature of 15Cr-ODS steels, which is defined as the tensile stress equal to the Mises stress of 359 MPa, is 800 °C, while that is 550 °C for F82 H.

Table 1 ODS steels developed in each country.

Country	Alloys (compositions)
Belgium	DT2906:Fe-13Cr-1.5Mo-2.9Ti-0.6Y_2O_3, DT2203Y05:Fe-13Cr-5Mo- 2.2Ti-0.3O-0.5Y_2O_3)
China	K7:Fe-13Cr-1.1Ti-0.2Mo-2W-0.39Y_2O_3
Europe	ODS EUROFER:Fe-9Cr-1.1W-0.2V-0.14Ta -0.3 (0.5)Y_2O_3
Japan	Fe-9(12)Cr-0.12C-2W-0.2(0.3)Ti -0.35(0.23)Y_2O_3, 14-15Cr-2W-0.25Ti-0.35Y_2O_3
USA	MA957:Fe-14Cr-0.9Ti-0.3Mo-0.25Y_2O_3, 12CrY1:Fe-12.4Cr-.25Y_2O_3, 14CrYWTi:Fe-14.3Cr-3W-0.39Ti-0.25 Y_2O_3

3.2 Creep properties

Figure 2 shows Larson-Miller diagram of the ODS steels [36] with a value of 25 as the coefficient parameter to gather creep data measured between 600 and 900 °C. The data of the F/M steel, F82H, and SUS316L are also

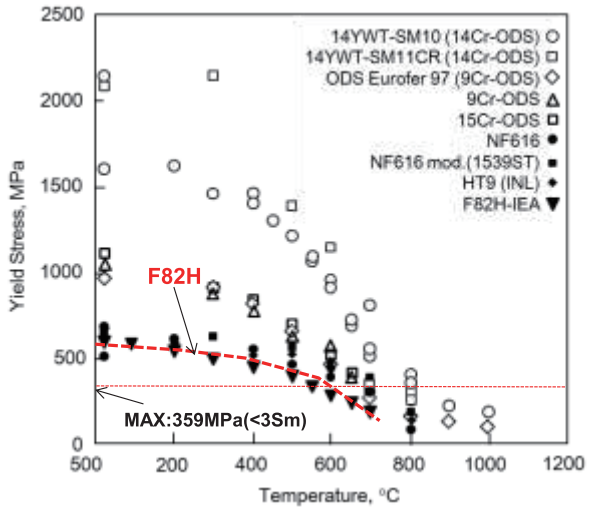

Fig. 1 F/M steels (● ■ ◆), 9Cr-ODS steels (◇ △), 15Cr-ODS steels (○ □ ◘), RAFM steel (F82H: ▼) [32–40].

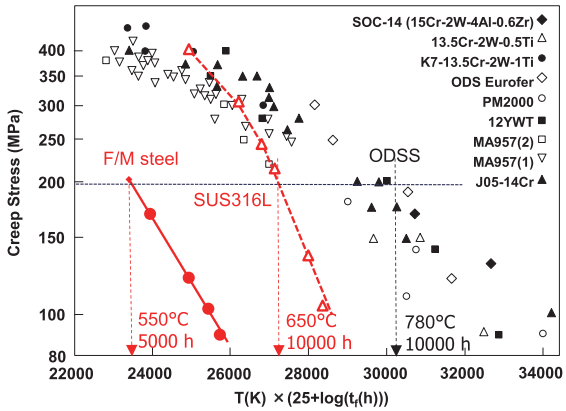

Fig. 2 Larson-Miller diagram of the ODS steels [36].

plotted in the figure for comparison. Although the data of the ODS steels are widely distributed in a band because the data was obtained from various sorts of ODS steels, it is clear that the creep stress of the ODS steels is much higher than those of F82H. Figure 2 indicates that the creep strength of 200 MPa is available for ODS steels at 780 °C with 10,000 h of rapture time, while the test temperature and rapture time of F82H is 550 °C and 5000 h, respectively.

The extrusion process leads to extremely elongated fine grains parallel to the extruding direction, which results in the anisotropy in the strength. This is particularly detrimental in the hoop direction of the claddings as a primary stress mode in fission gas-pressurized fuel pins [39]. In the case of ODS martensitic steels, the ferrite to austenite transformation caused by austenitization heat treatment makes the elongated grains be adequately equiaxed. However, in the case of ODS ferritic steels, the matrix has no this kind of transformation. Therefore, the recrystallization treatment is necessary to reduce the anisotropy and to relieve its internal stress. Thus, the creation of equiaxed grains has been considered to be critical for the development of ODS ferritic steel claddings. The recrystallization processing has been considered to be an effective way to overcome the anisotropy. Related report [39] showed that after a suitable recrystallization, the creep rupture strength of 12Cr-ODS ferritic steels in the hoop direction was significantly improved, resulting from breaking of the elongated grains and generating more equiaxed grains by means of recrystallization processes.

Sakasegawa *et al.* investigated the feature of the creep rupture of an ODS steel which raptured along pre-powder boundaries where so called void coalescence happened to form large voids that played a role as nucleation site of ductile rupture. The important is that the ductile rupture occurs in steady creep region without appearance of the third stage of tertiary creep [41], although the rapture time is much longer than the conventional ferritic steels.

3.3 Fatigue

The research on low cycle fatigue properties of ODS steels is very limited. Ukai *et al.* [42] investigated the low cycle fatigue properties of 9Cr ODS martensitic and 12Cr ODS ferritic steel at high temperatures. They summarized that the 9Cr-ODS and 12Cr-ODS steels have similar fatigue properties, and the ODS steels show superior fatigue life under the high cycle conditions compared to the conventional ferritic steels such as Mod. 9Cr–1Mo steel. They also confirmed a high strength after fatigue tests of ODS steels, that is, cyclic stability, i.e. no cyclic softening [43].

3.4 Fracture toughness

Byun *et al.* produced two ODS steels (NFAs) designated as 9YWTV-PM1 and 9YWT-PM2, with nominal components: Fe-9Cr-2W-0.4Ti-0.2V-0.12C-0.3Y_2O_3 and Fe-9Cr-2W-0.4Ti-0.2V-0.05C-0.3Y_2O_3, respectively [44]. In their previous research on fracture mechanism using the NFA-14YWT, it was found that the low-energy grain boundary decohesion in fracture process at a high temperature (>200 °C) resulted in low fracture toughness [45,46]. Lately, efforts have been devoted to explore an integrated process to enhance grain boundary strength. Isothermal annealing (IA) and controlled rolling (CR) treatments in two-phase region were used to enhance diffusion across the interfaces and boundaries. The PM2 alloy after CR treatments showed high fracture toughness (K_{JQ}) at represented temperatures: 240 - 280 MPa$\sqrt{m}$ at room temperature and 160 - 220 MPa$\sqrt{m}$ at 500 °C. This indicates that the target fracture toughness of over 100 MPa$\sqrt{m}$ has been well achieved in the temperature range of nuclear application. It was also confirmed that the CR treatment on 9YWTV-PM2 resulted in its high fracture toughness similar to or even higher than those of the conventional F/M steels such as HT9 and NF616.

4. Corrosion in Supercritical Pressurized Water

Corrosion is another critical issue for blanket structural material. Corrosion tests were carried out for several materials in a supercritical pressurized water (SCPW) condition to compare the corrosion behavior. The tests were carried out at 500 °C for 600 h at a pressure of 25 MPa in SCPW dissolved with 8 ppm of oxygen, and the weight gain was measured. The results were shown in Fig. 3, indicating that the weight gain considerably depended on Cr content. As expected, F82H that contains 8 wt.% Cr shows the maximum weight gain among the materials. The 9Cr-ODS steel without addition of Al also shows a large weight gain similar to F82H, while the 15 wt.% Cr ODS steel shows the smallest value in comparison to the other candidate alloys, such as nickel or iron based stainless steels

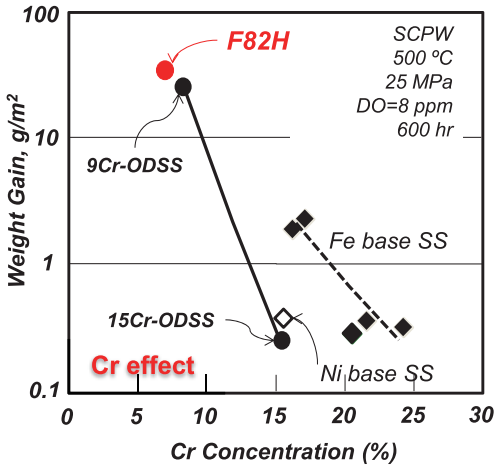

Fig. 3 Weight gains of each material after corrosion test in SCPW [15].

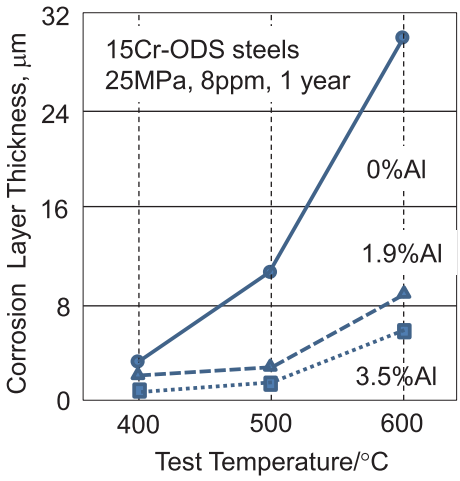

Fig. 4 The dependence of corrosion layer thickness on the amount of Al addition and test temperature. The values are estimated from the experimental data for 1000 h.

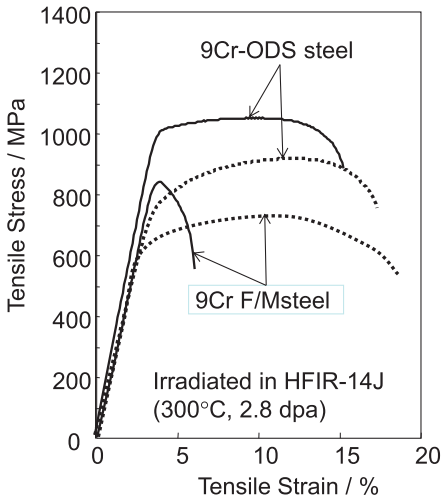

Fig. 5 The stress-strain curves of 9Cr steels with and without oxide dispersion tested at room temperature after irradiation at 300 °C to 2.8 dpa. (solid:irr., dotted:unirr.)

with Cr contents higher than 15 wt.%. Figure 3 indicates that the corrosion rate of the 15Cr-ODS steel is two orders of magnitude smaller than F82H. Considering the application to water cooled advanced blanket, the elevation of water temperature above the critical point is required to increase the thermal efficiency. However, F82H is not adequate for the application to SCPW cooled blanket with keeping long lifetime.

As for the effects of the other alloying elements than Cr, it was also shown that an addition of Al is effective to reduce the weight gain of the ODS steels and the effect becomes significant with decreasing Cr content from 19 to 15 wt.% [47, 48]. The estimated corrosion layer thickness as a function of temperature and Al contents is shown in Fig. 4 for ODS ferritic steels with different amount of Al addition after exposure to SCPW for 1 year. It was found that the corrosion layer thickness of the ODS steel significantly depended on the temperature. At 400 °C, the Al addition to ODS steel increases slightly their corrosion resistance. However, the contribution of Al to the corrosion resistance is increased at higher temperatures. Especially at 600 °C, the effect of Al is remarkable. After exposure to SCPW at 600 °C for 1 year, the oxide thickness of Al-added ODS steel was about 5 μm, indicating that the addition of 3.5 wt.%Al to 15Cr-ODS steel improves its corrosion resistance at higher temperatures, although Al is not adequate for fusion application from the view of reduced activation. The previous research on the chemical analysis and XRD measurements of the corrosion layer revealed that the layer of Al-free 15Cr-ODS steels consists of three parts, Fe_2O_3 outer layer, Fe_3O_4 middle one and $(Fe, Cr)_3O_4$ inner one, after the test for 300 h at 510 °C in SCPW dissolved with 8 ppm oxygen [49]. In the Al-added ODS steels, a thin alumina layer was formed at the most inner region of the multi-corrosion layers [47–49].

5. Radiation Tolerance

5.1 Tensile properties

Nano-sized oxide particles dispersion resulted in a unique behavior under irradiation. Generally, irradiation induces hardening and embrittlement in metallic materials. Figure 5 shows the stress-strain curves of 9Cr F/M steel and 9Cr-ODS steel before and after neutron irradiation at 300 °C up to 2.8 dpa in the HFIR in Oak Ridge National Laboratory. The 9Cr F/M steel shows a large irradiation hardening of about 200 MPa and the hardening is accompanied by a drastic reduction of tensile elongation showing no work hardening or homogeneous deformation. The loss of elongation is interpreted in terms of the irradiation enhancement of localized deformation. The localized deformation is well known as channel deformation in neutron irradiated metals, where once the dislocations move over the irradiation-induced defects, the following moving dislocations can move easily because the defects are absorbed by the leading dislocations. Since localized plastic deformation accelerates necking or ductile fracture, the total elongation is reduced. In the case of the ODS steel, however, irradiation-induced hardening is not accompanied by the reduction of total elongation. This could be due to the suppression of localized deformation caused by the activation of many dislocation sources by oxide particles. Since the fine dispersion of oxide particles play a role as obstacles to dislocation motion, the leading dislocation can be trapped at the particles and a back stress is applied to suppress the continuous dislocation source activation. Therefore, in the ODS steel, a number of dislocation sources are activated in the whole tensile specimen, and homogeneous deformation occurs.

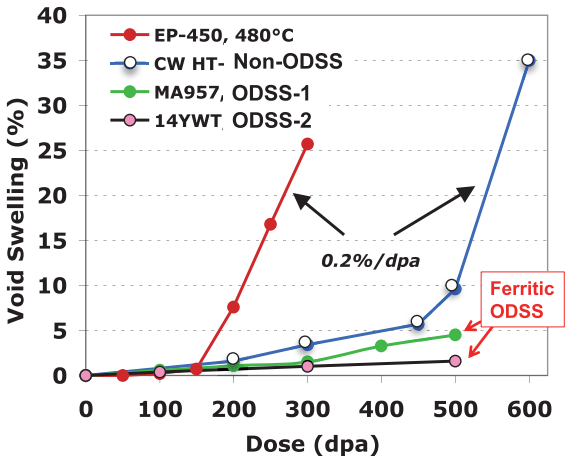

Fig. 6 Void swelling in F/M steels and MA957 [50].

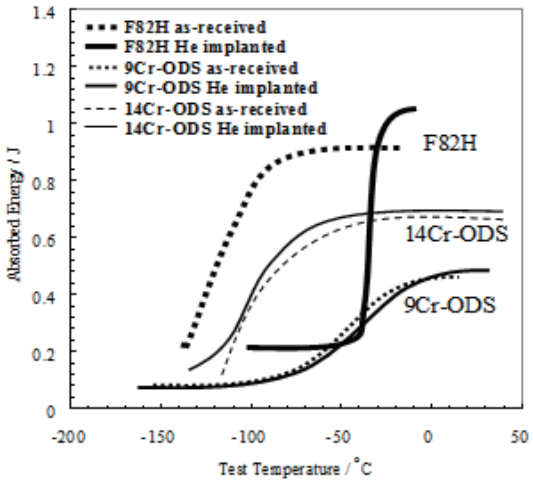

Fig. 7 Charpy impact absorbed energy vs. temperature curves [25].

5.2 Swelling

Void swelling behavior up to several hundreds dpa was investigated by Toroczko *et al.* with use of a van de Graf electrostatic accelerator of heavy ions with an external injector of 1.8 MeV Cr^{3+} ions [50]. Three different steels were irradiated: HT-9 and MA957 at 450 °C, and 480 °C for EP-450 (Fig. 6). The EP-450, which is a ferritic steel, shows a linear increase in the swelling beyond 150 dpa at the swelling rate of 0.2%/dpa. The HT-9 tempered martensitic steel shows good resistance to swelling up to 400 dpa, then shows a rapid increase in swelling at the similar rate with EP-450. The swelling of MA957, however, is still small even after the irradiation up to 500 dpa, which is considered to be due to large trapping capacity of defects in the microstructures of the ODS steel, such as fine oxide particles, grain boundaries and dislocations [50].

5.3 Helium embrittlement

Transmutation helium effects on fracture behavior will be critical for integrity of fusion structural materials. Implantation helium effect on the impact fracture behavior was investigated for F82 H, 9Cr-ODS and 14Cr-ODS steels. Results of the impact tests with using sub-sized specimens ($1.5 \times 1.5 \times 20\,mm^3$) of these steels are shown in Fig. 7 [25]. Materials were implanted with helium ions of 40 MeV with a penetration depth of 0.4 mm at the V-notch region. The Charpy impact energy vs. temperature curves of F82H before and after He implantation revealed that the DBTT was shifted by 70 °C by 1000 appm He implantation. The Vickers hardness test results indicate a slight hardening ($\Delta Hv = 40$) in the He-implanted area of these specimens. A SEM micrograph of the He-implanted specimens revealed that intergranular fracture surface was observed only from the bottom of the notch to a depth of about 400 μm which corresponded to the He-implanted region. No grain boundary fracture was observed in the range beyond the He-implantation. Not so many researches had dealt with the microstructural characterization of He-implanted specimens, except for that by Takahashi *et al.* They examined the microstructure of F82H after 1000 appm He implantation at 550 °C, and showed that large He bubbles were formed both in the grains and at grain boundaries [51]. Thus, intergranular fracture was presumably initiated by crack formation at He bubbles on grain boundaries.

The fracture mode in both the He-implanted and un-implanted regions of the 9Cr-ODS steel was cleavage, and no intergranular fracture was observed. The hardness of the He-implanted area appeared to be decreased.

The DBTT of both the as-received and He-implanted 14Cr-ODS steel was −100 °C. No fracture mode change due to He implantation was observed. The DBTT of 14Cr-ODS steel did not change upon the He implantation but a slight decrease of hardness ($\Delta Hv = -15$) was observed in the He-implanted area. From the view point of microstructure, the 9Cr-ODS steel has martensitic structure and the 14Cr-ODS steel has ferritic structure. Both specimens have fine and dense oxide particles [27, 52]. Yutani *et al.*, showed that a number of small He bubbles were observed at the fine oxide particles after ion irradiation [53]. These results revealed that the fine and dense oxide particles in the ODS steels had enough trapping capacity of He up to 1000 appm at around 600 °C.

6. Coupling RAFM and ODS Steels

Technological advancement of structure materials is indispensable for the realization of the high efficiency blanket beyond the DEMO reactor. The maximum acceptable operation temperature for the RAFM steel has been predicted as 550 °C based on the creep property. Using finite element method, the stress distribution in the first wall of water cooled TBM was evaluated by two-dimensional thermo-mechanical analysis [54], which indicated that the highest TRESCA stress of 359 MPa appeared at the same

place as the highest temperature. This stress value was evaluated to satisfy the 3Sm value for F82H. According to this TRESCA criteria, the highest temperature for the ODS steel can be evaluated to be 780 °C from Figs. 1 and 2. Furthermore, the corrosion behavior should be taken into account in consideration of the lifetime of blankets. At first, it should be recognized that the weight gain of high-Cr steel in SCPW remarkably depends on Cr content. The corrosion rate of the ODS steel is almost similar to that of RAFM steel when Cr content is 9 wt.% [55–57]. According to the previous research [58], the corrosion layer thickness could be estimated to be 600 and 5 μm for RAFM steel and 15Cr-ODS steel, respectively, at 500 °C for 1 year.

As for helium embrittlement, it was reported that there was a critical amount of helium content at grain boundaries to induce grain boundary embrittlement [59]. In F/M steels, no helium effects were observed up to 600 appm of helium-implantation. However, after implantation to 1000 appm of He, F82H showed a definite intergranular cracking, indicating that 1000 appm He is an enough amount to cause intergranular cracking of F82H, while the ODS steel never showed susceptibility to the embrittlement up to 1000 appmHe. As for the effect of irradiation on the tensile elongation, the RAFM steel showed a significant loss of total elongation but the ODS steel did show no loss of elongation. The above mentioned is summarized in Table 2.

Thus, ODS steels possess rather high materials performance than RAFM steels. However, it is difficult to fabricate massive products of ODS steel because of the limitation of the mechanical alloying process. It can be said that both F/M steels and ODS steels are used as a coupling component where ODS steels are used to face severer environment and RAFM steels are for production of huge structural container.

It is recognized that early realization of the nuclear fusion energy is essential for acceleration of fusion reactor development. However, thermal efficiency of power plant is also important for the reduction of future energy source consumption. For the progress in fusion science and technology, aiming high level of target may push people forward to realization of fusion reactors.

Table 2 Comparison of materials performance between RAFM and ODS steels.

Materials		RAF Steel (F82H)	ODS Steel (15Cr-ODSS)
Thermal Efficiency	Operation temp.	Max. temp. allowable = 539 °C Max. stress allowable = 359 MPa (<3Sm)	Max. temp. allowable = 780 °C Max. stress allowable = 359 MPa (<3Sm)
Lifetime	Creep rapture time	10 khr (180 MPa, 550 °C)	10 khr (180 MPa, 780 °C)
	Corrosion rate (oxide thickness)	0.6 mm (500 °C, 1 year)	0.003 mm (500 °C, 1 year)
	Acceptable helium content	< 600 appm (40 dpa)	> 1000 appm (65 dpa)
	Irr. Embritt. at RT	A large loss of elongation	No loss of elongation
Water Cooling Systems		High Temp. Water 15 MPa, 309 °C	SCP Water 25 MPa, 502 °C

7. Dissimilar Joint (FSW)

Dissimilar joining of ODS ferritic steel and RAFM steel is necessary to expand the flexible design margin and get benefits from each material in a functional way. Numerous researches have shown that conventional melting welding techniques are inadequate for ODS alloys, because the melting process results in the agglomeration of nano-sized oxide particles, which causes degradation of performance of ODS alloys [60–62]. In addition, melting weld process of F82H, a martensitic steel, is accompanied by the phase transformation that causes significant changes in material performance [63–65]. The solid state joining technique, friction stir welding (FSW), has been shown to be an appropriate method for welding both ODS steels and F82H steels [66, 67].

In FSW process, the stir zone (SZ) of the joint suffers drastic thermomechanical effects imposed by the stirring tool, and undergoes complicated microstructural evolutions. Chung [67] reported that defect-free F82H joints could be successfully fabricated by FSW, without formation of neither the δ ferrite nor inter-metallic compounds. However, complicated phase transformations and the grain structure changes were found in SZ. Several researches [64–66, 68] on microstructural evolution during FSW process of ODS ferritic steels reached an agreement that the recrystallization occurred in the ODS SZ.

Figure 8 presents grain morphologies of BM and SZ in the ODS part of the dissimilar joint. Comparing the elongated and preferentially orientated grains in the ODS BM, the SZ grains exhibit an equiaxed shape and random orientations. As the welding temperature is about 980 °C during

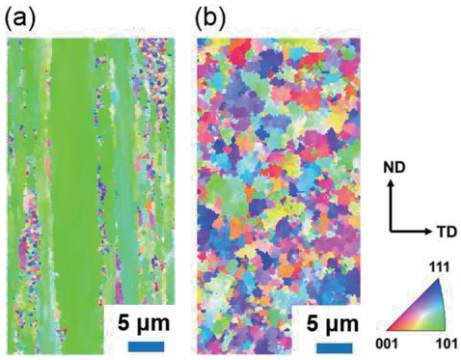

Fig. 8 Grain characteristics of ODS side of the dissimilar joint: (a) IPF of BM, (b) IPF of SZ [72].

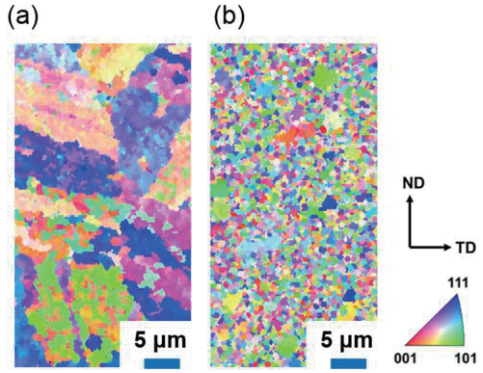

Fig. 9 Grain characteristics ofF82H side of the dissimilar joint: (a) IPF of BM, (b) IPF of SZ [72].

the FSW process, the 15Cr-ODS steel stays in a single α phase, and no phase transformation could occur. The remarkable changes in the grain morphology in ODS SZ are strong evidence that the SZ grains have experienced recrystallization. However, the 15Cr-ODS ferritic steel usually needs heat treatment at about 1300 °C for more than 1 h for recrystallization [69]. Contrarily, the recrystallization during the FSW process happens quite faster even at much lower temperature. It indicates that the recrystallization in FSW should be achieved by a specific mechanism. Fonda *et al.*, [70, 71] and Han *et al.* [65, 69, 72] investigated the recrystallization behavior during FSW of ODS steel. The common findings are that recrystallized grains in the SZ are formed by the continuous dynamic recrystallization, in which subgrains are recrystallized not by the nucleation/growth mechanism but by plastic flow mechanism.

Significant changes in grain morphologies of BM and SZ can also be found on F82H side of the joint, as shown in Fig. 9. However, the mechanism of microstructural evolutions in the F82H part is quite different from that in the ODS part. The evolution mechanism in F82H SZ is identified as phase transformations, since the welding temperature exceeds the AC_1 (840 °C) of F82H steel. During the heating process of FSW, the martensite grains in F82H SZ can transform to the austenite grains. After the stir tool was removed from the welded area, γ–α transformation happened in the sequential cooling process. As the cooling rate is quite high, during the γ–α transformation, martensitic grains with fine grain size and high hardness value (about 475 Hv in F82H SZ) can be generated, while F82H BM comprises much coarser grains and processes a lower hardness value (235 Hv).

8. Summary

RAFM steels have been considered as candidates for structure material of ITER-TBM. On the other hand, their materials performances are insufficient in considering the application to advanced blankets bearing high efficiency and long lifetime for commercial reactors. It is thought that the application of ODS steels is effective in advancing blanket technology, particularly in the case that high thermal efficiency and long lifetime are demanded. ODS steels surpass RAFM steels in several materials performance, and the ODS steels raise the operation temperature of the blanket in comparison to the RAFM steels. On the other hand, a difficulty is the limit in the productivity of ODS steels by means of powder metallurgy processing, and the ODS steels might be unfavorable in the manufacturing huge components where a large quantity of materials are necessary.

Therefore, in consideration of merits and demerits of both the RAFM steel and ODS steel, it is vital to use both steels according to a way of thinking the right material in the right place. The supporting structure body of a blanket needs a large quantity of steel, and F82H meets the requirement. The design of a blanket using both RAFM steel and ODS steel may impose high thermal efficiency with the extension of lifetime by using rather small amount of ODS steel. In the coupling use of RAFM steel and ODS steel, joining technology development becomes indispensable. The research on the effect of irradiation on the properties of the joints is another issue.

Acknowledgements

The authors appreciate many thanks to collaborators including staffs of Institute of Advanced Energy, Kyoto University, students of Graduate School of Energy Science, Kyoto University and research group members on Super ODS steels R&D.

Present study includes the result of "R&D of corrosion resistant super ODS steel for highly efficient nuclear systems" entrusted to Kyoto University by the Ministry of Education, Culture, Sports, Science and Technology of Japan (MEXT) and "R&D of high-Cr ODS steels for practical application to LWR" by the Ministry of Economy, Trade and Industry (METI).

[1] A. Moslang, C.R. Physique **9**, 457 (2008).
[2] F.W. Wiffen and R.T. Santoro, Proceedings of the Topical Conference on Ferritic Alloys for Use in Nuclear Energy Technologies, AIME, New York (1984).
[3] M. Tamura, H. Hayakawa, H. Tanimura, A. Hishinuma and T. Kondo, J. Nucl. Mater. **141-143**, 1067 (1986).
[4] H. Tanigawa *et al.*, J. Nucl. Mater. **417**, 9 (2011).
[5] A. Kimura *et al.*, J. Nucl. Mater. **367-370**, 60 (2007).
[6] A. Kimura, M. Narui and H. Kayano, J. Nucl. Mater. **191-194**, 879 (1992).
[7] A. Kimura and H. Matsui, J. Nucl. Mater. **212-215**, 701 (1994).
[8] A. Kimura, T. Morimura, M. Narui and H. Matsui, J. Nucl. Mater. **233-237**, 319 (1996).
[9] T. Liao, O.N. Bedoya-Martínez and G. Roma, J. Phys. Chem. C **114**, 22691 (2010).
[10] L.L. Snead, T. Nozawa, Y. Katoh, T.-S. Byun, S. Kondo and D.A. Petti, J. Nucl. Mater. **371**, 329 (2007).
[11] Y. Katoh, L.L. Snead, C.M. Parish and T. Hinoki, J. Nucl. Mater. **434**, 141 (2013).

[12] S.J. Zinkle *et al*., J. Nucl. Mater. **258-263**, 205 (1998).
[13] R.J. Kurtz *et al*., J. Nucl. Mater. **329-333**, 47 (2004).
[14] T. Muroga *et al*., J. Nucl. Mater. **307-311**, 547 (2002).
[15] A. Kimura *et al*., J. Nucl. Mater. **417**, 176 (2011).
[16] L. Hsiung, M. Fluss, S. Tumey, J. Kuntz, B. El-Dasher, M. Wall, B. Choi, A. Kimura, F. Willaime and Y. Serruys, J. Nucl. Mater. **409**, 72 (2011).
[17] T. Kaito *et al*., J. Nucl. Mater. **386-388**, 294 (2009).
[18] S. Ukai, S. Mizuta, M. Fujiwara, T. Okuda and T. Kobayashi, J. Nucl. Sci. Technol. **39**, 778 (2002).
[19] S. Ukai, T. Okuda, M. Fujiwara, T. Kobayashi, S. Mizuta and H. Nakashima, J. Nucl. Sci. Technol. **39**, 872 (2002).
[20] R. Kasada, H. Takahashi, H. Kishimoto, K. Yutani and A. Kimura, Mater. Sci. Forum **654-656**, 2791 (2010).
[21] J. Isselin, R. Kasada and A. Kimura, J. Nucl. Sci. Technol. **48**(2), 169 (2011).
[22] N. Okuda, R. Kasada and A. Kimura, J. Nucl. Mater. **386-388**, 974 (2009).
[23] H. Kishimoto, R. Kasada, O. Hashitomi and A. Kimura, J. Nucl. Mater. **386-388**, 533 (2009).
[24] J. Chen, M.A. Pouchon, A. Kimura, P. Jung and W. Hoffelner, J. Nucl. Mater. **386-388**, 143 (2009).
[25] A. Hasegawa *et al*., J. Nucl. Mater. **386-388**, 241 (2009).
[26] A. Kimura *et al*., J. Nucl. Mater. **307-311**, 521 (2002).
[27] H.S. Cho, A. Kimura, S. Ukai and M. Fujiwara, J. Nucl. Mater. **329-333**, 387 (2004).
[28] N.A. Azarenkov *et al*., Nanostructural materials in the nuclear engineering, J. Kharkiv National Univ., 1041 (2013) p.19-28.
[29] A. Kimura *et al.*, J. Nucl. Mater. **417**, 176 (2011).
[30] R.L. Klueh *et al.*, J. Nucl. Mater. **307-311**, 455 (2002).
[31] R.L. Klueh *et al.*, J. Nucl. Mater. **341**, 103 (2005).
[32] T. Yoshitake, Y. Abe, N. Akasaka, S. Ohtsuka, S. Ukai and A. Kimura, J. Nucl. Mater. **329-333**, 342 (2004).
[33] S. Ohtsuka *et al.*, J. Nucl. Mater. **329-333**, 372 (2004).
[34] S. Ohtsuka *et al.*, J. Nucl. Mater. **351**, 241 (2006).
[35] T. Sawazaki *et al.*, J. Nucl. Mater. **442**, S169 (2013).
[36] A. Steckmeyer, V.H. Rodrigo, J.M. Gentzbittel, V. Rabeau and B. Fournier, J. Nucl. Mater. **426**, 182 (2012).
[37] S. Ukai, *Metal, Ceramic and Polymeric Composites for Various Uses*, ed. Cuppoletti, J., Chapter 14 (InTech) ISBN: 978-953-307-353-8 (2011).
[38] H. Sakasegawa *et al*., J. Nucl. Mater. **367-370**, 185 (2007).
[39] S. Ukai *et al.*, J. Nucl. Sci. Technol. **39**, 872 (2002).
[40] S. Ohtsuka *et al.*, J. Nucl. Mater. **367-370**, 160 (2007).
[41] H. Sakasegawa *et al.*, J. Nucl. Mater. **373**, 82 (2008).
[42] S. Ukai *et al.*, J. Nucl. Mater. **367-370**, 234 (2007).
[43] P. Marmy and T. Kruml, J. Nucl. Mater. **377**, 52 (2008).
[44] T.S. Byun *et al*., J. Nucl. Mater. **449**, 290 (2014).
[45] T.S. Byun *et al*., J. Nucl. Mater. **407**, 78 (2010).
[46] J.H. Kim *et al.*, J. Nucl. Mater. **407**, 143 (2010).
[47] H.S. Cho, A. Kimura, S. Ukai and M. Fujiwara, J. of ASTM International **2**(7), 111 (2005).
[48] H.S. Cho, H. Ohkubo, N. Iwata, A. Kimura, S. Ukai and M. Fujiwara, Fusion Eng. Des. **81**, 1071 (2006).
[49] A. Kimura, H.S. Cho, N. Toda, R. Kasada, K. Yutani, H. Kishimoto, N. Iwata, S. Ukai and M. Fujiwara, J. Nucl. Sci. Technol. **44**(3), 323 (2007).
[50] M.B. Toloczko, F.A. Garner, V.N. Voyevodin, V.V. Bryk, O.V. Borodin, V.V. Mel'nychenko and A.S. Kalchenko, J. Nucl. Mater. **453**, 323 (2014).
[51] H. Takahashi and A. Kimura, unpublished work.
[52] S. Ukai *et al*., J. Nucl. Sci. Technol. **39**, 778 (2002).
[53] K. Yutani, H. Kishimoto, R. Kasada and A. Kimura, J. Nucl. Mater. **367-370**, 423 (2007).
[54] M. Enoeda *et al*., Fusion Eng. Des. **81**, 1–7, 415 (2006).
[55] I. Kubena *et al*., J. Nucl. Mater. **424**, 101 (2012).
[56] H. Hadraba *et al*., J. Nucl. Mater. **411**, 112 (2011).
[57] T.R Allen *et al*., Proc. the 12th Int'l Conf. on Environmental Degradation of Materials in Nuclear Power System, (2005) p.1397-1407.
[58] F. Kano *et al*., Review, No.12, 62 (2004) (in Japanese).
[59] A. Kimura, R. Kasada, R. Sugano, A. Hasegawa and H. Matsui, J. Nucl. Mater. **283-287**, 827 (2000).
[60] B.W. Baker, T.R. McNelley and L.N. Brewer, Mater. Sci. Eng. A **589**, 217 (2014).
[61] R. Lindau, M. Klimenkov, U. Jäntsch, A. Möslang and L. Commin, J. Nucl. Mater. **416**, 22 (2011).
[62] H.J.K. Lemmen, J. Mater. Science **42**, 5286 (2007).
[63] F. Legendre *et al*., J. Nucl. Mater. **386-388**, 537 (2009).
[64] S. Noh *et al*., J. Nucl. Mater. **417**, 245 (2011).
[65] W.T. Han *et al*., Science and Technology of Welding and Joining **16**, 690 (2011).
[66] W. Han *et al*., Mater. Trans. JIM **53**, 390 (2012).
[67] Y.D. Chung, H. Fujii, Y. Sun and H. Tanigawa, Mater. Sci. Eng. A **528**, 5812 (2011).
[68] K. Yabuuchi *et al*., Mater. Sci. Eng. A **595**, 291 (2014).
[69] W. Han *et al.*, J. Nucl. Mater. **455**, 46 (2014).
[70] R.W. Fonda *et al*., Scr. Mater. **51**, 243 (2004).
[71] R.W. Fonda *et al*., Scr. Mater. **58**, 343 (2008).
[72] W-Han *et al*., Scr. Mater. **105**, 2 (2015).